New Layered Materials: Syntheses, Structures, and Optical Properties of $K_2TiCu_2S_4$, $Rb_2TiCu_2S_4$, $Rb_2TiAg_2S_4$, $Cs_2TiAg_2S_4$, and $Cs_2TiCu_2Se_4$

Fu Qiang Huang and James A. Ibers*

Department of Chemistry, Northwestern University, 2145 Sheridan Road, Evanston, Illinois 60208

Received November 29, 2000

The new compounds $K_2TiCu_2S_4$, $Rb_2TiCu_2S_4$, $Rb_2TiAg_2S_4$, $Cs_2TiAg_2S_4$, and $Cs_2TiCu_2Se_4$ have been synthesized by the reactions of A_2Q_3 (A = K, Rb, Cs; Q = S, Se) with Ti, M (M = Cu or Ag), and Q at 823 K. The compounds $Rb_2TiCu_2S_4$, $Cs_2TiAg_2S_4$, and $Cs_2TiCu_2Se_4$ are isostructural. They crystallize with two formula units in space group $P4_2/mcm$ of the tetragonal system in cells of dimensions $a = 5.6046(4)$ Å, $c = 13.154(1)$ Å for $Rb_2TiCu_2S_4$, $a = 6.024(1)$ Å, $c = 13.566(4)$ Å for $Cs_2TiAg_2S_4$, and $a = 5.852(2)$ Å, $c = 14.234(5)$ Å for $Cs_2TiCu_2Se_4$ at 153 K. Their structure is closely related to that of $Cs_2ZrAg_2Te_4$ and comprises $^2_\infty[TiM_2Q_4^{2-}]$ layers, which are separated by alkali metal atoms. The $^2_\infty[TiM_2Q_4^{2-}]$ layer is anti-fluorite-like with both Ti and M atoms tetrahedrally coordinated to Q atoms. Tetrahedral coordination of Ti^{4+} is rare in the solid state. On the basis of unit cell and space group determinations, the compounds $K_2TiCu_2S_4$ and $Rb_2TiAg_2S_4$ are isostructural with the above compounds. The band gaps of $K_2TiCu_2S_4$, $Rb_2TiCu_2S_4$, $Rb_2TiAg_2S_4$, and $Cs_2TiAg_2S_4$ are 2.04, 2.19, 2.33, and 2.44 eV, respectively, as derived from optical measurements. From band-structure calculations, the optical absorption for an $A_2TiM_2Q_4$ compound is assigned to a transition from an M d and Q p valence band (HOMO) to a Ti 3d conduction band.

Introduction

The extensive recent work[1−11] on CdQ (Q = S, Se, Te) illustrates that nanoscale materials show different physical properties (e.g., increased band gap energy, decreased melting point, and enhanced photocatalytic activity[12,13]) from those of their bulk-phase counterparts. These differences arise from the disruption of extended, three-dimensional bonding networks found in the binary bulk phases. Many techniques have been used to reduce the dimensions of these materials in order to change electronic band gaps.[14−19] There have also been some attempts to obtain the same electronic effects by reducing the dimensionality of the structures.[20−23] Related two-dimensional ternary cadmium chalcogenides $A_2Cd_3Q_4$ (A = alkali metal) are known.[20,21,24] The band gaps of CdQ and $A_2Cd_3Q_4$ differ, but they are both determined by the highest occupied molecular orbitals (HOMO) consisting of Cd 4d orbitals and Q p orbitals and the lowest unoccupied molecular orbitals (LUMO) consisting mainly of Cd 5s orbitals. If Cd atoms are substituted by two different kinds of transition metal atoms, such as a group 4 or 5 metal atom (M) and a group 11 or 12 metal atom (M′), then the band gap of the material may be determined by the HOMO of mainly M′ d and Q p orbitals and the LUMO of mainly M d orbitals. Therefore, the band gap can be modified and controlled by the appropriate substitution. We illustrate this here with the substitution of Ti and Cu or Ag for Cd to form the two-dimensional layered compounds $K_2TiCu_2S_4$, $Rb_2TiCu_2S_4$, $Rb_2TiAg_2S_4$, $Cs_2TiAg_2S_4$, and $Cs_2TiCu_2Se_4$. The structures of these compounds are related to those of $A_2Cd_3Q_4$,[20,24] but, as expected, their band gaps are different.

Experimental Details

Syntheses. The following reagents were used as received: K (Aldrich, 98+%), Rb (Aldrich, 98+%), Cs (Aldrich, 98+%), Ti (Reacton, 99.9%), Cu (Alfa, 99.999%), Ag (Alfa, 99.5%), S (Alfa,

(1) Bube, R. H. *Photoconductivity of Solids*; John Wiley & Sons: New York, 1960.
(2) Rouxel, J., Ed. *Crystal Chemistry and Properties of Materials with Quasi-one-dimensional Structures*; Physics and Chemistry of Materials with Low-Dimensional Structures; Series B, Quasi-One-Dimensional Materials; D. Reidel: Dordrecht, Netherlands, 1986.
(3) Chen, B.-H.; Eichhorn, B.; Peng, J.-L.; Greene, R. L. *J. Solid State Chem.* **1993**, *103*, 307−313.
(4) Ohtani, T.; Sano, Y.; Yokota, Y. *J. Solid State Chem.* **1993**, *103*, 504−513.
(5) Lee, J.-G.; Chan, S.; Ramanujachary, K. V.; Greenblatt, M. *J. Solid State Chem.* **1996**, *121*, 332−338.
(6) Wilson, J. A.; DiSalvo, F. J.; Mahajan, S. *Adv. Phys.* **1975**, *24*, 117−201.
(7) DiSalvo, F. J. *Surf. Sci.* **1976**, *58*, 297−311.
(8) DiSalvo, F. J.; Rice, T. M. *Phys. Today* **1979**, *32*, 32−38.
(9) Tremel, W. *Angew. Chem., Int. Ed. Engl.* **1992**, *31*, 217−220.
(10) Ansari, M. A.; Ibers, J. A. *Coord. Chem. Rev.* **1990**, *100*, 223−266.
(11) Roof, L. C.; Kolis, J. W. *Chem. Rev.* **1993**, *93*, 1037−1080.
(12) Kanatzidis, M. G.; Huang, S.-P. *Coord. Chem. Rev.* **1994**, *130*, 509−621.
(13) Kanatzidis, M. G. *Comments Inorg. Chem.* **1990**, *10*, 161−195.
(14) Rossetti, R.; Hull, R.; Gibson, J. M.; Brus, L. E. *J. Chem. Phys.* **1985**, *82*, 552−554.
(15) Dev, S.; Ramli, E.; Rauchfuss, T. B.; Stern, C. L. *J. Am. Chem. Soc.* **1990**, *112*, 6385−6386.
(16) Alivisatos, A. P. *J. Phys. Chem.* **1996**, *100*, 13226−13239.
(17) Spanhel, L.; Anderson, M. A. *J. Am. Chem. Soc.* **1990**, *112*, 2278−2284.
(18) Weller, H. *Angew. Chem., Int. Ed. Engl.* **1993**, *32*, 41−53; *Angew. Chem.* **1993**, *105*, 43.
(19) Herron, N.; Wang, Y.; Eckert, H. *J. Am. Chem. Soc.* **1990**, *112*, 1322−1326.
(20) Axtell, E. A., III; Liao, J.-H.; Pikramenou, Z.; Kanatzidis, M. G. *Chem.—Eur. J.* **1996**, *2*, 656−666.
(21) Axtell, E. A., III; Liao, J.-H.; Pikramenou, Z.; Park, Y.; Kanatzidis, M. G. *J. Am. Chem. Soc.* **1993**, *115*, 12191−12192.
(22) Albrecht-Schmitt, T. E.; Ibers, J. A. *Angew. Chem., Int. Ed. Engl.* **1997**, *36*, 2010−2011.
(23) Albrecht-Schmitt, T. E.; Cody, J. A.; Hupp, J. T.; Ibers, J. A. *Inorg. Chem.* **1995**, *34*, 5101−5102.
(24) Narducci, A. A.; Ibers, J. A. *J. Alloys Compd.* **2000**, *306*, 170−174.

10.1021/ic001346d CCC: $20.00
Published on Web 04/18/2001

99.5%), and Se (Alfa, 99.5%). A_2Q_3 (A = K, Rb, Cs; Q = S, Se), the reactive flux employed in the reaction,[25] was synthesized by the stoichiometric reaction of the elements in liquid NH_3. The compounds $K_2TiCu_2S_4$, $Rb_2TiCu_2S_4$, $Rb_2TiAg_2S_4$, $Cs_2TiAg_2S_4$, and $Cs_2TiCu_2Se_4$ were prepared by the reactions of 1.5 mmol of A_2Q_3, 1.0 mmol of Ti, 2.0 mmol of M (M = Cu or Ag), and 3.0 mmol of Q. The reactants were loaded into fused-silica tubes under an argon atmosphere in a glovebox. These tubes were sealed under a 10^{-4} Torr atmosphere and then placed in a computer-controlled furnace. The samples were heated to 823 K at 1 K/min, kept at 823 K for 2 days, slowly cooled at 0.10 K/min to 373 K, and then cooled to room temperature. The reaction mixtures were washed free of alkali-metal chalcogenides with dimethylformamide and then dried with acetone. The major products from these reactions were orange-red, orange, or yellow plates or blocks, along with a few similarly colored needles. Yields for these products are about 90%, based on Ti. Analysis of the plates and blocks with an EDX-equipped Hitachi S-4500 SEM showed the presence of A, Ti, M, and Q in the molar ratio of about 2:1:2:4. Analysis of the needles gave a molar ratio A:Ti:Q of approximately 1:1:5; unit cell determinations confirmed that these needles are $A_4Ti_3Q_{14}$, which consists of $^1_\infty[Ti_3(Q)_2(Q_2)_6^{4-}]$ chains separated by A atoms.[26] The compounds $K_2TiCu_2S_4$, $Rb_2TiCu_2S_4$, $Rb_2TiAg_2S_4$, $Cs_2TiAg_2S_4$, and $Cs_2TiCu_2Se_4$ are very stable in air.

Structure Determinations. Single-crystal X-ray diffraction data were collected with the use of graphite-monochromatized Mo Kα radiation (λ = 0.71073 Å) at 153 K on a Bruker Smart-1000 CCD diffractometer.[27] The crystal-to-detector distance was 5.023 cm. Crystal decay was monitored by recollecting 50 initial frames at the end of data collection. Data were collected with a scan of 0.3° in ω in groups of 606, 606, and 606 frames at ϕ settings of 0°, 180°, and 240° for $Rb_2TiCu_2S_4$, $Cs_2TiAg_2S_4$, and $Cs_2TiCu_2Se_4$. The exposure time was 15 s/frame. The collection of intensity data on the Bruker diffractometer was carried out with the program SMART.[27] Cell refinement and data reduction were carried out with the use of the program SAINT,[27] and face-indexed absorption corrections were performed numerically with the use of the program XPREP.[28] The program SADABS[27] was then employed to make incident beam and decay corrections. In addition, unit cell data were collected for $K_2TiCu_2S_4$ and $Rb_2TiAg_2S_4$.

The structures of $Rb_2TiCu_2S_4$, $Cs_2TiAg_2S_4$, and $Cs_2TiCu_2Se_4$ were solved with the direct methods program SHELXS and refined with the full-matrix least-squares program SHELXL of the SHELXTL-PC suite of programs.[29] Each final refinement included anisotropic displacement parameters and a secondary extinction correction. Additional experimental details are given in Table 1 and in Supporting Information. Table 2 presents selected bond distances.

UV−Vis Diffuse Reflectance Spectroscopy. A Cary 1E UV−visible spectrophotometer with a diffuse reflectance accessory was used to measure the diffuse reflectance spectra over the range 350 nm (~3.54 eV) to 900 nm (~1.38 eV) at 293 K on the compounds $K_2TiCu_2S_4$, $Rb_2TiCu_2S_4$, $Rb_2TiAg_2S_4$, and $Cs_2TiAg_2S_4$.

Extended Hückel Calculations. Calculations were performed on tetrahedral TiS_4^{4-} and CuS_4^{7-} fragments, the defect $^2_\infty[Cu_3S_4^{5-}]$ and nondefect $^2_\infty[Cu_2S_2^{2-}]$ layers in LaCuOS,[30] and the $^2_\infty[TiCu_2S_4^{2-}]$ layer in $RbTiCu_2S_4$ with the use of the YAeHMOP package.[31−33] These calculations were each carried out on only one layer in the corresponding unit cell. The parameters used for the Ti, Cu, and S orbitals are listed in Table 3.

Table 1. Crystal Data and Structure Refinement for $Rb_2TiCu_2S_4$, $Cs_2TiAg_2S_4$, and $Cs_2TiCu_2Se_4$[a]

	$Rb_2TiCu_2S_4$	$Cs_2TiAg_2S_4$	$Cs_2TiCu_2Se_4$
fw	474.16	657.70	756.64
space group	$P4_2/mcm$	$P4_2/mcm$	$P4_2/mcm$
a (Å)	5.6046(4)	6.024(1)	5.852(2)
c (Å)	13.154(1)	13.566(4)	14.234(5)
V (Å^3)	413.19(6)	492.3(2)	487.4(3)
Z	2	2	2
T (K)	153(2)	153(2)	153(2)
λ	0.71073	0.71073	0.71073
ρ_{calc} (g/cm^3)	3.811	4.437	5.156
μ (cm^{-1})	186.59	127.83	273.36
$R(F)^b$ ($F_o^2 > 2\sigma(F_o^2)$)	0.022	0.027	0.033
$R_w(F_o^2)^c$ (all data)	0.071	0.071	0.094

[a] The tetragonal unit cell constants (a, c) are 5.5467(8) and 12.758(3) Å for $K_2TiCu_2S_4$ and 5.959(1) and 13.208(2) Å for $Rb_2TiAg_2S_4$. [b] $R(F) = \sum||F_o| - |F_c||/\sum|F_o|$. [c] $R_w(F_o^2) = [\sum w(F_o^2 - F_c^2)^2/\sum wF_o^4]^{1/2}$, $w^{-1} = \sigma^2(F_o^2) + (0.04F_o^2)^2$ for $F_o^2 > 0$; $w^{-1} = \sigma^2(F_o^2)$ for $F_o^2 \le 0$.

Table 2. Selected Distances (Å) for $Rb_2TiCu_2S_4$, $Cs_2TiAg_2S_4$, and $Cs_2TiCu_2Se_4$

Distance	$Rb_2TiCu_2S_4$	$Cs_2TiAg_2S_4$	$Cs_2TiCu_2Se_4$
A−Q ×4	3.4457(8)	3.568(1)	3.666(1)
A−Q ×4	3.4451(8)	3.706(1)	3.667(1)
Ti−Q ×4	2.2775(8)	2.294(1)	2.3994(9)
M−Q ×4	2.3665(6)	2.5568(9)	2.4732(9)

Table 3. Atomic Parameters Used for the Extended Hückel Calculations

element	orbital	H_{ii} (eV)	ζ_1	ζ_2	C_1	C_2
Cu	4s	−11.40	2.20	2.30	0.5933	0.5744
	4p	−6.06	2.20			
	3d	−14.00	5.95			
Ti	4s	−8.970	1.0750	1.400	0.4206	0.7839
	4p	−5.440	1.0750			
	3d	−10.81	4.550			
S	3s	−20.00	2.122			
	3p	−14.00	1.827			

TB-LMTO Calculations. First-principles self-consistent local density approximation (LDA)[34] calculations of the electronic structures of $Rb_2TiCu_2S_4$ and $Cs_2TiCu_2Se_4$ were performed with the use of the tight-binding (TB) linear muffin-tin orbital (LMTO) method in the atomic sphere approximation (ASA), including the combining correction.[35−37] This method splits the crystal space into overlapping atomic spheres (Wigner-Seitz spheres) whose radii are chosen to fill completely the crystal volume. In the present calculations, space-filling is achieved without overlapping atomic spheres with one another by more than 15%, without overlapping atomic spheres with interstitial spheres by more than 20%, and without overlapping interstitial spheres with one another by more than 25%. All k-space integrations were performed with the tetrahedron method.[38,39] Within the irreducible Brillouin zone, calculations for the $Rb_2TiCu_2S_4$ compound used the 12 irreducible k-points that, because of the high symmetry, come from 32 k-points. The basis sets consisted of 5s, 5p, and 4d for Rb; 6s, 6p, and 5d for Cs; 4s, 4p, and 3d for Ti; 4s, 4p, and 3d for Cu; 3s and 3p for S; 4s and 4p for Se. E p-d states were downfolded by means of Löwdin's technique.[38,39]

(25) Sunshine, S. A.; Kang, D.; Ibers, J. A. *J. Am. Chem. Soc.* **1987**, *109*, 6202−6204.
(26) Huang, F. Q.; Ibers, J. A. *Inorg. Chem.* **2001**, *40*, 2346−2351.
(27) SMART Version 5.054 Data Collection and SAINT-Plus Version 6.02A Data Processing Software for the SMART System; Bruker Analytical X-Ray Instruments, Inc.: Madison, WI, 2000.
(28) Sheldrick, G. M. SHELXTL DOS/Windows/NT Version 5.10; Bruker Analytical X-Ray Instruments, Inc.: Madison, WI, 1997.
(29) Sheldrick, G. M. SHELXTL PC Version 5.0 An Integrated System for Solving, Refining, and Displaying Crystal Structures from Diffraction Data; Siemens Analytical X-Ray Instruments, Inc.: Madison, WI, 1994.
(30) Palazzi, M. *C. R. Acad. Sci., Ser. 2* **1981**, *292*, 789−791.
(31) Landrum, G. Yet Another Extended Hückel Molecular Orbital Package (YAeHMOP) Version 2.0, 1997.
(32) Hoffmann, R. *J. Chem. Phys.* **1963**, *39*, 1397−1412.
(33) Whangbo, M.-H.; Hoffmann, R. *J. Am. Chem. Soc.* **1978**, *100*, 6093−6098.
(34) Hedin, L.; Lundqvist, B. I. *J. Phys. Chem. Solids* **1971**, *4*, 2064−2083.
(35) Andersen, O. K. *Phys. Rev. B* **1975**, *12*, 3060−3083.
(36) Andersen, O. K.; Jepsen, O. *Phys. Rev. Lett.* **1984**, *53*, 2571−2574.
(37) Jepsen, O.; Andersen, O. K. *Z. Phys. B* **1995**, *97*, 35−47.
(38) Lambrecht, W. R. L.; Andersen, O. K. *Phys. Rev. B* **1986**, *34*, 2439−2449.
(39) Jepsen, O.; Andersen, O. K. *Solid State Commun.* **1971**, *9*, 1763−1767.

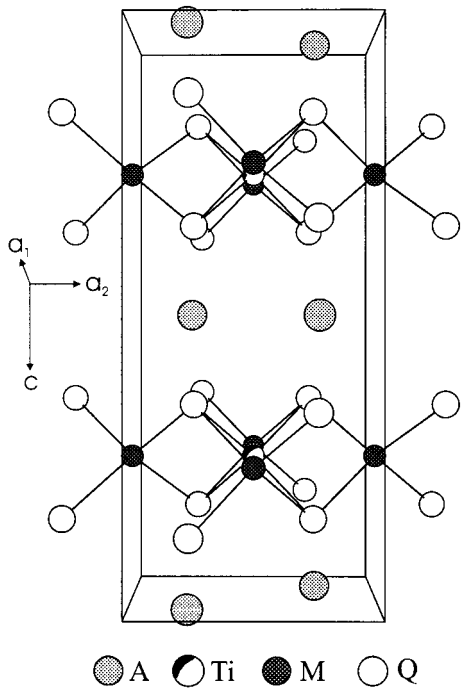

Figure 1. Unit cell of $A_2TiM_2Q_4$ viewed down [010].

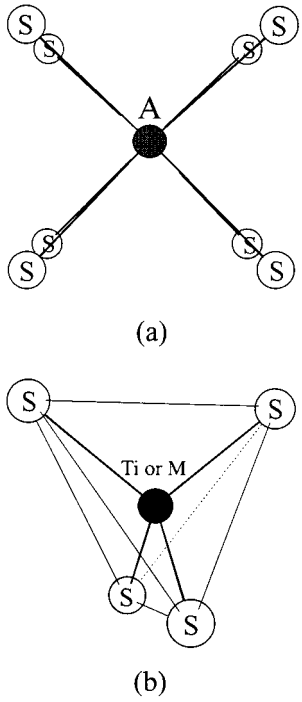

Figure 2. The coordination environments of (a) atom A and (b) atom Ti or atom M.

Results and Discussion

Description of the Structures. The structure of the isostructural compounds $Rb_2TiCu_2S_4$, $Cs_2TiAg_2S_4$, and $Cs_2TiCu_2Se_4$ is displayed in Figure 1. This structure is very similar to that of $Cs_2ZrAg_2Te_4$ (orthorhombic, *C*222).[40] The present structure of $A_2TiM_2Q_4$ consists of $^2_\infty[TiM_2Q_4^{2-}]$ layers stacked along the *c* axis, and separated by A atoms. Each A atom is coordinated to a rectangular prism of eight Q atoms (Figure 2a). The $^2_\infty[TiM_2Q_4^{2-}]$ layer projected down [001] is shown in Figure 3. The dashed lines form a square net in the (110) plane. The large square is the unit cell of the layer. It contains one Ti, two M, and four Q atoms and consists of four dashed squares. A Ti atom and the two M atoms are located at three of the four corners of each square, and the other corner is vacant. Q atoms are in turn at the up and down cap positions of squares resulting in TiQ_4 and MQ_4 tetrahedra (Figure 2b). To achieve charge balance (Ti^{4+}, M^+, Q^{2-}) the square net of $^2_\infty[TiM_2Q_4^{2-}]$ in $A_2TiM_2Q_4$ has to contain vacant positions. The $^2_\infty[TiM_2Q_4^{2-}]$ layer is of the defect anti-fluorite-like type, for if all the corners of the squares were occupied by metal atoms then the layer would be anti-fluorite-like. Such anti-fluorite-like layers are very common and are found, for example, in the $ThCr_2Si_2$ (or $BaAl_4$) structure type.[41]

It is interesting to compare the structure of $A_2TiM_2Q_4$ with those of various $A_2Cd_3Q_4$ compounds. The $A_2Cd_3Q_4$ compounds are members of a large $A_2M_3Q_4$ family (A = K, Rb, Cs; M = Mn, Co, Zn, Cd, Hg; Q = S, Se, Te).[20,24,42-45] The known $A_2Cd_3Q_4$ compounds crystallize in three distinct structure types:

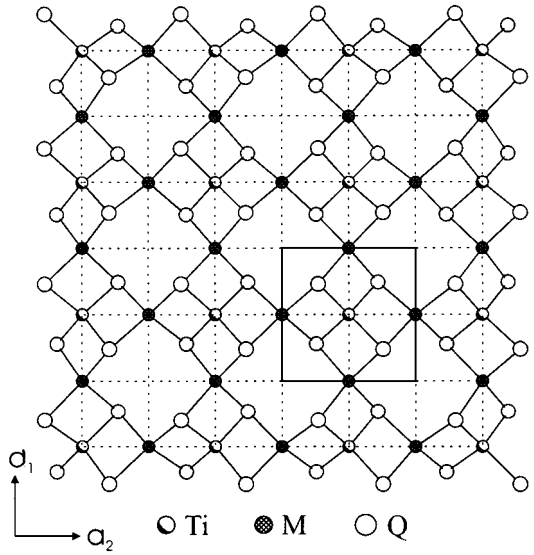

Figure 3. The $^2_\infty[TiM_2Q_4^{2-}]$ layer projected down [001]. Here and in Figure 4 the large box is the unit cell in the layer.

$K_2Cd_3S_4$ (space group *Pnma*),[20] $Cs_2Zn_3S_4$ (space group *Ibam*),[42] and $K_2Zn_3O_4$ (space group *C*2/*c*).[46] $Cs_2Cd_3Te_4$ belongs to the $Cs_2Zn_3S_4$ type, $Rb_2Cd_3Te_4$ belongs to the $K_2Zn_3O_4$ type,[24] and the others are of the $K_2Cd_3S_4$ type,[20] as shown in Figure 4. They are all composed of $^2_\infty[Cd_3Q_4^{2-}]$ layers separated by alkali metal atoms. In all these compounds Cd atoms are coordinated tetrahedrally to four Q atoms and the Q atoms are connected to three Cd atoms, except that there are some connected to two Cd atoms and to four Cd atoms in $Rb_2Cd_3Te_4$ (Figure 4b). The $^2_\infty[Cd_3Q_4^{2-}]$ layer in the $K_2Cd_3S_4$ type structure is composed of defect cubes, and Cd atoms are in a triangular net (Figure 4c). The layers in $Cs_2Cd_3Te_4$ and $Rb_2Cd_3Te_4$ are both defect anti-

(40) Pell, M. A.; Ibers, J. A. *J. Am. Chem. Soc.* **1995**, *117*, 6284−6286.
(41) Villars, P., Calvert, L. D., Eds. *Pearson's Handbook of Crystallographic Data for Intermetallic Phases*, 2nd ed.; ASM International: Materials Park, OH, 1991; Vol. 1.
(42) Bronger, W.; Hendriks, U.; Müller, P. *Z. Anorg. Allg. Chem.* **1988**, *559*, 95−105.
(43) Klepp, K. O. *J. Alloys Compd.* **1992**, *182*, 281−288.
(44) Bronger, W.; Hardtdegen, H.; Kanert, M.; Müller, P.; Schmitz, D. *Z. Anorg. Allg. Chem.* **1996**, *622*, 313−318.
(45) Wu, E. J.; Ibers, J. A. *Acta Crystallogr., Sect. C: Cryst. Struct. Commun.* **1997**, *C53*, 993−994.
(46) Baier, R.; Hoppe, R. *Z. Anorg. Allg. Chem.* **1987**, *551*, 163−172.
(47) Pankove, J. I. *Optical processes in semiconductors*; Dover: New York, 1975.

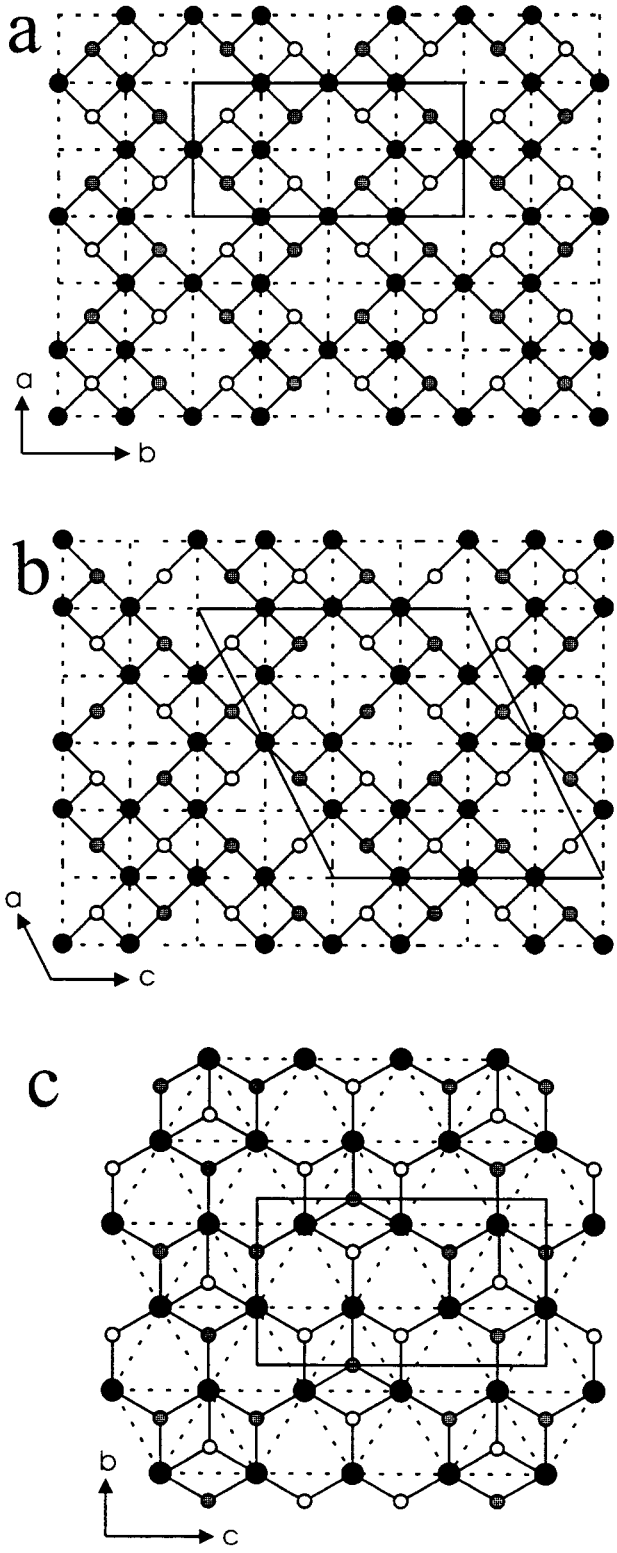

Figure 4. The ideal layers of (a) $^2_\infty[Cd_3Q_4^{2-}]$ in $Cs_2Cd_3Te_4$, (b) $^2_\infty[Cd_3Q_4^{2-}]$ in $Rb_2Cd_3Te_4$, and (c) $^2_\infty[Cd_3Q_4^{2-}]$ in $K_2Cd_3Te_4$. The larger black filled circles represent Cd atoms, the smaller open circles represent the Q atoms above the Cd net, and the gray filled circles represent the Q atoms below the Cd net.

fluorite-like with one-quarter of the corners of the square nets vacant, but these layers differ from one another and from the $^2_\infty[TiM_2Q_4^{2-}]$ layer in the present compounds (Figures 4a,b and 3). The unit cells are projected onto the layers, as shown in the large boxes in these figures. These boxes comprise four squares for $^2_\infty[TiM_2Q_4^{2-}]$, eight squares for $^2_\infty[Cd_3Te_4^{2-}]$ in $Cs_2Cd_3Te_4$, and sixteen squares for $^2_\infty[Cd_3Te_4^{2-}]$ in $Rb_2Cd_3Te_4$. As the symmetry of the crystal system decreases from tetragonal $A_2TiM_2Q_4$ to orthorhombic $Cs_2Cd_3Te_4$ to monoclinic $Rb_2Cd_3Te_4$, the MQ_4 tetrahedra distort more. If we take the difference between the longest and shortest M−Q distances as a measure of this distortion, then we have 0 Å in $A_2TiM_2Q_4$, 0.127(2) Å in $Cs_2Cd_3Te_4$, and 0.245(2) Å in $Rb_2Cd_3Te_4$.

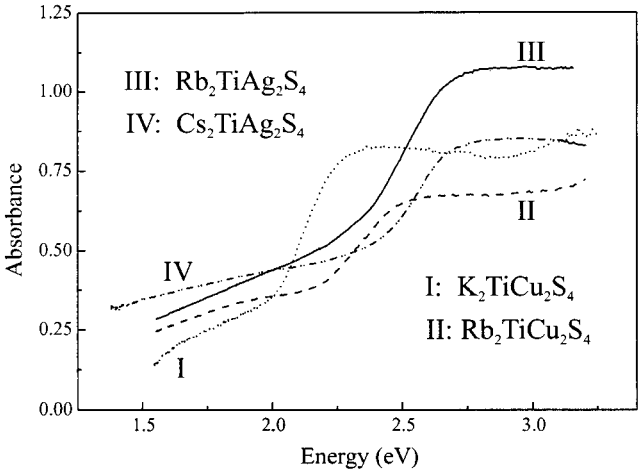

Figure 5. Diffuse reflectance spectra of $K_2TiCu_2S_4$, $Rb_2TiCu_2S_4$, $Rb_2TiAg_2S_4$, and $Cs_2TiAg_2S_4$.

Table 4. Band Gaps in Selected Cadmium Chalcogenides

compound	band gap (eV)	ref	compound	band gap (eV)	ref
$K_2Cd_3S_4$	2.75	20	$Rb_2Cd_3Te_4$	2.30	24
$Rb_2Cd_3S_4$	2.92	20	$Cs_2Cd_3Te_4$	2.48	24
$K_2Cd_3Se_4$	2.36	20	CdS[a]	2.44	47
$Rb_2Cd_3Se_4$	2.37	20	CdSe[a]	1.74	47
$K_2Cd_3Te_4$	2.26	20	CdTe[a]	1.5	47

[a] Bulk phase.

Table 5. Colors, Band Gaps, and Cell Constants for $K_2TiCu_2S_4$, $Rb_2TiCu_2S_4$, $Rb_2TiAg_2S_4$, $Cs_2TiAg_2S_4$, and $Cs_2TiCu_2Se_4$

compound	color	cell constants (*a*, *c*) (Å)	band gap (eV)
$K_2TiCu_2S_4$	orange	5.5467(8), 12.758(3)	2.04
$Rb_2TiCu_2S_4$	orange	5.6046(4), 13.154(1)	2.19
$Cs_2TiCu_2Se_4$	orange-red	5.852(2), 14.234(5)	not measd[a]
$Rb_2TiAg_2S_4$	yellow	5.959(1), 13.208(2)	2.33
$Cs_2TiAg_2S_4$	yellow	6.024(1), 13.566(4)	2.44

[a] It was difficult to separate $Cs_2TiCu_2Se_4$ from $Cs_4Ti_3Se_{14}$.

Band Gaps and Their Origins. The diffuse reflectance spectra of $K_2TiCu_2S_4$, $Rb_2TiCu_2S_4$, $Rb_2TiAg_2S_4$, and $Cs_2TiAg_2S_4$ are shown in Figure 5. From these spectra optical band gaps of 2.04, 2.19, 2.33, and 2.44 eV, respectively, have been derived. The band gaps for a series of cadmium chalcogenides are presented in Table 4. The optical absorption in these cadmium chalcogenides was assigned to mainly a Q^{2-} valence band to mainly a Cd^{2+} conduction band.[20] In these compounds, within a given structure type the one containing the heavier chalcogen atom has the lower band gap. The band gap in the $A_2Cd_3Q_4$ (Q = S, Se) compounds (Table 4) is also affected by the alkali metal (A). As the size of the A atom increases, so does the unit cell layer area and the band gap. The colors, unit cell constants, and band gaps of the $A_2TiM_2Q_4$ compounds are listed in Table 5. The same trend of band gap with increasing size of A is observed.

The origin of the optical absorptions in the present compounds has been investigated through theoretical calculations on $Rb_2TiCu_2S_4$. Extended Hückel calculations have been performed

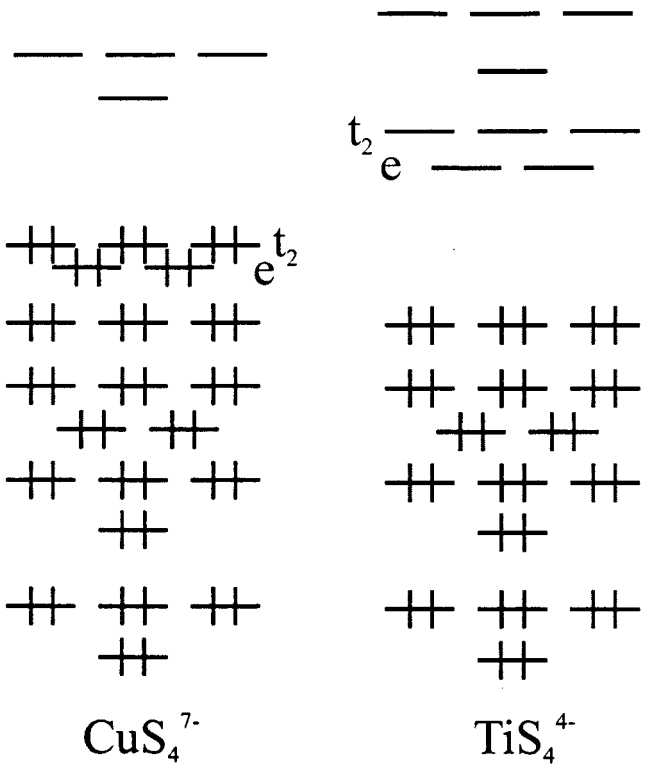

Figure 6. The orbital filling of CuS_4^{7-} and TiS_4^{4-}.

Table 6. Some Selected Calculated Results around the Fermi Surface

	HOMO (eV)	LUMO (eV)	gap[a] (eV)
CuS_4^{7-}	−12.829	−3.221	9.608
TiS_4^{4-}	−13.782	−8.287	5.495
$^2_\infty[Cu_3S_4^{5-}]$	−12.332	−6.496	4.836
$^2_\infty[Cu_2S_2^{2-}]$	−12.124	−7.548	4.572
$^2_\infty[TiCu_2S_4^{2-}]$	−12.505	−8.087	4.418
$^2_\infty[TiCu_2S_4^{2-}]$			1.70[b]
$^2_\infty[TiCu_2Se_4^{2-}]$			1.52[b]

[a] Gap = LUMO − HOMO. [b] TB-LMTO calculation.

on the hypothetical tetrahedral CuS_4^{7-} and TiS_4^{4-} molecular fragments, the two-dimensional hypothetical defect $^2_\infty[Cu_3S_4^{5-}]$ layer, and the $^2_\infty[TiCu_2S_4^{2-}]$ layer. The Cu−S and Ti−S distances were taken as 2.37 and 2.30 Å, respectively. The $^2_\infty[Cu_3S_4^{5-}]$ and $^2_\infty[TiCu_2S_4^{2-}]$ layers were extracted from the structures of LaCuOS[30] and $Rb_2TiCu_2S_4$, respectively. For the molecular tetrahedral CuS_4^{7-} and TiS_4^{4-} fragments, the orbital fillings are shown in Figure 6. In these tetrahedral coordination environments, five 3d atomic orbitals (AO) are split into a typical "two below three" (e below t_2), with few contributions to make bonds with neighboring S atoms. In CuS_4^{7-}, nonbonding Cu 3d (t_2) and S 3p orbitals occupy the HOMOs and antibonding orbitals (mainly Cu 4s and some S 3p) make up the LUMOs. For the TiS_4^{4-} fragment, five 3d AOs are not occupied, the HOMOs are filled mainly by S 3p, and the LUMOs consist mainly of the e orbitals of Ti 3d. The values of the energy levels around the Fermi surface are listed in Table 6. The energy level of the HOMO in going from molecular CuS_4^{7-} to the perfect $^2_\infty[Cu_2S_2^{2-}]$ layer increases only slightly from −12.829 to −12.124 eV whereas the LUMO decreases more drastically, −3.221 to −7.548 eV, because of the larger dispersion of Cu 4s versus Cu 3d orbitals. Therefore, the energy gap decreases from 9.608 eV for CuS_4^{7-} to 4.572 eV for $^2_\infty[Cu_2S_2^{2-}]$. Conceptually, if the size of the A atom is infinite, the "layer" consists of isolated MS_4 tetrahedra. Thus the larger band gap for CuS_4^{7-} compared with $^2_\infty[Cu_2S_2^{2-}]$ is consistent with the trend noted above of increasing band gap with increasing size of the A atom. The band structure of the $^2_\infty[TiCu_2S_4^{2-}]$ layer is illustrated in Figure 7. The energy levels of the HOMO and LUMO are −12.505 and −8.087 eV, respectively, which mainly consist of Cu 3d and S 3p AOs and Ti 3d AOs, respectively. The gap between HOMO and LUMO is 4.418 eV. The values of the energy levels for the HOMO and LUMO in $^2_\infty[TiCu_2S_4^{2-}]$ are very close to those for the HOMO in CuS_4^{7-} and for the LUMO in TiS_4^{4-}.

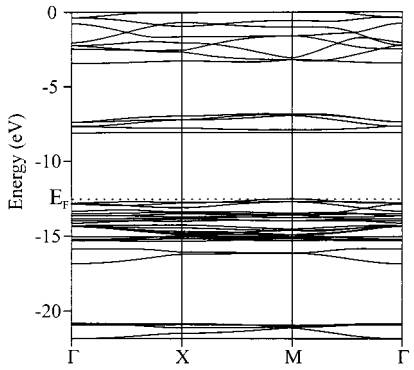

Figure 7. The band structure of the $^2_\infty[TiCu_2S_4^{2-}]$ layer in $Rb_2TiCu_2S_4$, where Γ, X, and M are (0,0,0), ($^1/_2$,0,0), and ($^1/_2$,$^1/_2$,0).

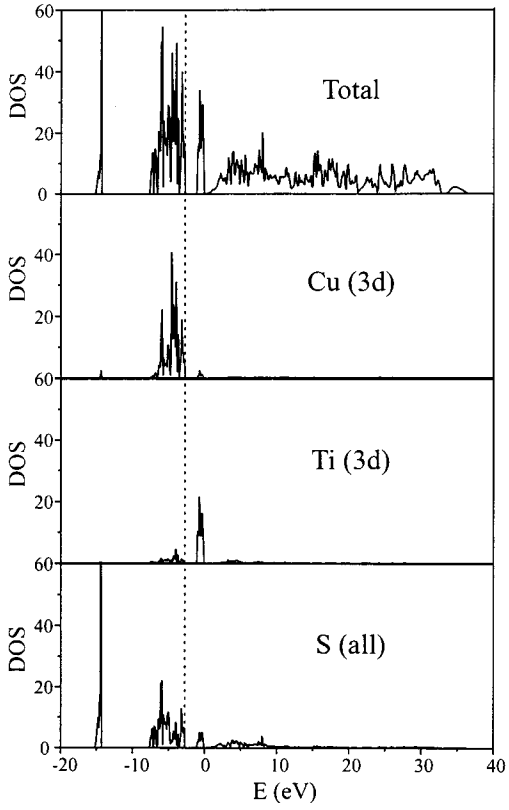

Figure 8. The DOS of all atoms, Cu (3d), Ti(3d), and S (all orbitals) in $Rb_2TiCu_2S_4$.

In order to analyze in detail the behavior of the orbitals around the Fermi surface, TB-LMTO calculations were performed on the entire structures of $Rb_2TiCu_2S_4$ and $Cs_2TiCu_2Se_4$. The calculated band gaps are 1.70 and 1.52 eV, respectively, the former being much closer to the experimental value of $Rb_2TiCu_2S_4$ (2.19 eV) than that estimated from extended Hückel calculations. The smaller band gap in $Cs_2TiCu_2Se_4$ results from the higher energy levels of Se 4p AOs in the HOMO. This

calculation again indicates that Cu 3d and Q p AOs and Ti 3d AOs dominate the energy bands around the Fermi surface, as shown in Figure 8. In these kinds of layered compounds that contain two different kinds of transition metal atoms, such as a group 4 or 5 metal atom (M) and a group 11 or 12 metal atom (M′), the band gaps of the materials are determined by the HOMO of mainly M′ d and Q p orbitals and the LUMO of mainly M d orbitals.

Acknowledgment. This research was supported by NSF Grant DMR97-09351. Use was made of the Central Facilities supported by the MRSEC program of the National Science Foundation (DMR00-76097) at the Materials Research Center of Northwestern University.

Supporting Information Available: Crystallographic files in CIF format for $Rb_2TiCu_2S_4$, $Cs_2TiAg_2S_4$, and $Cs_2TiCu_2Se_4$. This material is available free of charge via the Internet at http://pubs.acs.org.

IC001346D